Temperature Dependence of Gas Transport in Polymer Melts: Molecular Dynamics Simulations of CO_2 in Polyethylene

N. F. A. van der Vegt

Membrane Technology Group, P.O. Box 217, 7500 AE Enschede, The Netherlands

Received October 19, 1999; Revised Manuscript Received February 7, 2000

ABSTRACT: The temperature dependence of carbon dioxide transport in an amorphous polyethylene melt has been studied using molecular dynamics simulations. At elevated temperatures, we have found strong slope changes in the Arrhenius plots for the diffusion and the solubility coefficients of the penetrant, lowering the activation energy for diffusion and the apparent heat of solution. The thermal population of penetrant energy states was studied to explain these phenomena. At low temperatures, sparsely distributed low-energy sites in the matrix were found populated, which causes the diffusion process to be strongly activated. At high temperatures, thermally accessible sorption sites with energies higher than the aforementioned ones were observed in significantly increased numbers. Consequently, the activation zone for diffusion decreases, and the entropy of solution increases. With decreasing slope of the Arrhenius plot for diffusion, the diffusion mechanism gradually changes from "hopping diffusion" to "liquidlike" diffusion, in agreement with the observations of others on different polymer/penetrant systems.

1. Introduction

The permeability of gases dissolved in synthetic polymers is of substantial importance in several engineering processes. In gas-phase polymerization processes, the monomer has to diffuse through the polymer in order to reach the reactive site, which process affects the overall polymerization kinetics. The production of low-density engineering polymers, such as microcellular polymers produced by foaming polymer/gas mixtures in continuous extrusion processes, can only be controlled effectively if the sorption thermodynamics as well as the diffusivity of the physical or chemical blowing agent inside the polymer melt is well understood. For the use in gas separations, synthetic polymer membranes are always designed to maximize the permeability of one component while minimizing the permeabilities of all other components present in the gaseous feed mixture. Barrier materials, on the other hand, are usually designed to have low permeabilities to all gases.

These examples show that the knowledge of the permeability of polymers to gases is required at various thermodynamic conditions. Polymerization processes and the extrusion of polymer/gas mixtures are usually performed at high pressures and temperatures, whereas polymeric gas separation membranes are usually operative at moderate temperatures and pressures. The gas permeability at low temperatures and pressures has been determined for many polymers in the past.[1] Experimental determination of such properties at high-pressure and -temperature conditions is a considerably more difficult task, and consequently little knowledge is available on the permeability of polymers under these conditions.

One way to obtain the gas permeability at high temperatures would be to determine the temperature dependence of the permeability in a finite low-temperature window and extrapolate to temperatures outside this window using the obtained activation energies for permeation. Such an approach will only be successful if the molecular-scale mechanism for gas diffusion and gas sorption does not alter significantly over the temperature range being studied.

Molecular dynamics (MD) simulation studies have revealed this mechanism and have first been reported in the early 1990s.[2] From these studies, it was shown that gases diffuse through polymers in a sequence of activated jumps between neighboring locations ("hopping diffusion"). This motion pattern is brought about by the so-called Red Sea mechanism.[2,3] The gas molecule—or penetrant—is dissolved in a cavity of free volume (sorption site), which it is exploring during most of its time present in the polymer. These cavities, which exist in all amorphous polymers, remain at fixed positions at the time scale relevant for penetrant diffusion; only their size and shape fluctuate. The thermal fluctuations of polymer atoms, however, constantly create and destroy transient channels of free volume between neighboring cavities. When, by coincidence, the penetrant is at the right position at the right time having the right velocity, it can slip through such a channel into the neighboring cavity. The channel will next close behind it.

The hopping diffusion mechanism—which applies to both the glassy and rubbery states of the polymer—differs significantly from tracer diffusion in low molecular weight liquids, to which we shall refer as "liquidlike" diffusion. In sharp contrast to the motions of the polymers and penetrants in polymer/penetrant mixtures, the motion of the tracer molecules in low molecular weight liquids reaches the diffusive limit on a time scale comparable to that of the solvent molecules. As the motions of both molecules are comparable, the random walk trajectory of the tracer molecule evolves smoothly in space, because the motions of solvent molecules continuously create new positions for the tracer to move to. The large separation of time scales in polymer/penetrant systems—as compared to these tracer/solvent systems—is the fundamental origin of the difference between "hoppinglike" and "liquidlike" diffusion.

The separation of the aforementioned time scales becomes less distinct as soon as the polymer chain dynamics increases. Increasing the temperature can lead to a redistribution of sorption sites sufficiently

10.1021/ma991737f CCC: $19.00
Published on Web 03/25/2000

quick to cause the hopping mechanism to change into a liquidlike diffusion mechanism. Indeed, this was observed in a series of MD simulations performed on polyethylene (PE)[4] and atactic polypropylene (aPP)[5] with methane as a diffusant. These studies clearly revealed the diffusion at low temperatures to be limited by the number of sites available to the penetrant in the polymer matrix and by the distribution of intersite energy barriers. At high temperature, this picture was found to break down, and the diffusion mechanism could be characterized with a much broader spectrum of jump lengths, with jumps occurring more frequently. This mechanistic change resulted in a strong non-Arrhenius behavior for diffusion with decreased activation energies at the higher temperatures.

In this paper we will show that a similar transition occurs in a polyethylene melt with carbon dioxide as a diffusant. The main purpose of this work is to illustrate that the mechanistic changes in the penetrant permeation mechanism described above (refs 4 and 5) can be related to the characteristics of a quantitative function with a clear microscopic and thermodynamic significance, which is unique for the system under investigation. This function—the thermal population of penetrant-energy states in the polymer matrix—will be shown to shift toward energy regions occurring at high density in the polymeric matrix at the hoppinglike-to-liquidlike transition. In addition, it will be shown that the shift of energy states populated strongly affects both the enthalpy and the entropy of solution. We will show that the latter property causes an inflection in the Arrhenius plot of the solubility at exactly the temperature where the activation energy for diffusion decreases.

In section 2 of this paper we will describe the computational procedures that were used to calculate both sorption and diffusion coefficients. In section 3, we will discuss the details of our simulations. The results will be presented and discussed in section 4. In section 5, the conclusions will be summarized.

2. Computational Methods

(a) Penetrant Diffusion. The diffusion coefficient of penetrant molecules in polymers can be calculated from the slope of the penetrant mean-square displacement for long times. At these times normal (Einstein) diffusion is observed, and the mean-square displacement is a linear function of time:

$$D = \frac{1}{6}\lim_{t\to\infty}\frac{\mathrm{d}}{\mathrm{d}t}\langle(\mathbf{r}(t) - \mathbf{r}(0))^2\rangle \qquad (1)$$

In eq 1, D is the diffusion constant, t is time, $\mathbf{r}(t)$ is the position vector of the penetrant molecule in space at time t, and the brackets denote an ensemble average, which in the simulation is obtained from averaging over all penetrants in the system and all time origins $t = 0$. This equation only applies in the limit of large times, i.e., times at which the penetrant has performed enough jumps for its trajectory to become a random walk in the polymer structure. The minimum simulation time required to calculate a diffusion coefficient, say $D = 10^{-6}$ cm^2/s, can be estimated from the distance traveled by the penetrant in one diffusive jump. This distance typically amounts $l_{\mathrm{jump}} = 5-10$ Å.[2] With this diffusion coefficient and $l_{\mathrm{jump}} = 10$ Å one finds that the simulation time needed to observe a penetrant jump event equals $t = l_{\mathrm{jump}}^2/6D = 1.7$ ns. This time is comparable to the maximum time (1−10 ns) during which one can actually simulate the dynamics of fully atomistic systems on present-day computers. Diffusion coefficients of slower penetrants ($D < 10^{-6}$ cm^2/s) in, e.g., glassy polymers therefore cannot be obtained from direct application of eq 1 to the simulated penetrant trajectory. Coarse-grained simulation methods have been developed that allow the study of slower polymer/penetrant systems.[6,7] These methods allow to extend simulation times to macroscopic time scales (microseconds−milliseconds). In our system, however, the carbon dioxide diffusion coefficient is large enough ($>10^{-6}$ cm^2/s) to obtain accurate results when eq 1 is applied directly to the simulated trajectory.

(b) Penetrant Solubility. The solubility of a penetrant can be expressed as the penetrant number density in the polymer/gas mixture relative to the penetrant number density in the adjacent, equilibrium (ideal) gas phase. Once determined experimentally, this ratio, which we will refer to as the partition coefficient K, allows to compute the penetrant excess chemical potential μ_{ex} in the mixture according to[8]

$$K = \exp(-\mu_{\mathrm{ex}}/RT) \qquad (2)$$

where R is the gas constant and T is the absolute temperature. In molecular simulations at constant particle number, the composition of the polymer/gas mixture is fixed, and the partition coefficient is obtained by computing μ_{ex}. We use the Widom test-particle insertion method[9] for this purpose:

$$\exp(-\mu_{\mathrm{ex}}/RT) = \int_{-\infty}^{\infty}\mathrm{d}\Delta E\ \rho(\Delta E)\exp(-\Delta E/RT) \qquad (3)$$

The integral in eq 3 denotes the NVT ensemble average of the Boltzmann factor of the test-particle insertion energy ΔE. The normalized energy distribution, $\rho(\Delta E)$, is calculated in the MD simulation. During the course of the simulation many test-particle insertions are performed at different time frames and stored in a histogram, which after normalization yields $\rho(\Delta E)$. Under constant pressure and temperature conditions (NPT ensemble), this distribution must be weighted with the volume of the system to account for the volume fluctuations.[10] In this work, the test-particle-insertion method is applied to a pure or "dry" polymer system; hence, the Henry limit—or infinite dilution—partition coefficient is obtained. The method can also be applied to polymer samples with varying penetrant concentrations, which yields the full concentration dependence of the penetrant solubility,[10] but in practice is limited by the size of the penetrants that can be inserted. Free volume cavities in amorphous polymers are large enough to accommodate small-sized penetrants such as He, H_2, N_2, and O_2 without substantial distortions of the matrix, allowing to compute well-converged values of μ_{ex}.[11,12] Sorption of much larger penetrants will disrupt (swell) the matrix, causing attempts to compute μ_{ex} using test-particle insertions to fail. We have reported simulation studies using expanded ensembles to effectively study the sorption thermodynamics of highly condensable, large penetrants.[13]

In addition to the excess chemical potential (eq 3), the excess partial molar enthalpy h_{ex} of the penetrant can

be computed from $\rho(\Delta E)$:[10,14]

$$h_{ex} \cong \frac{\int_{-\infty}^{\infty} d\Delta E\ \rho(\Delta E)\Delta E\ \exp(-\Delta E/RT)}{\int_{-\infty}^{\infty} d\Delta E\ \rho(\Delta E)\ \exp(-\Delta E/RT)} \quad (4)$$

In the derivation of this formula, it has been assumed that the total energy of the system is not correlated with the energy of insertion of a test particle. The excess partial molar entropy, s_{ex}, is then obtained using

$$Ts_{ex} = h_{ex} - \mu_{ex} \quad (5)$$

We note at this point that h_{ex} is always negative; i.e., the energetically favorable polymer−penetrant interactions will always favor dissolution of the gas because the interactions between gas molecules in the adjacent ideal gas phase are negligible by definition. When both h_{ex} and s_{ex} do not depend on the temperature at which the polymer phase and the gas phase are at equilibrium, an Arrhenius-type relation can be written for the partition coefficient K, describing its full temperature dependence:

$$K = K_0 \exp(-h_{ex}/RT), \quad K_0 = \exp(s_{ex}/R) = \text{constant} \quad (6)$$

With h_{ex} being negative, this equation—under the above-mentioned condition—predicts that the partition coefficient always decreases if the temperature is increased. It is important to emphasize here that eq 6 was introduced for a polymer/gas mixture at constant composition. Hence, h_{ex} is the *differential* heat of solution. As in our simulations composition is kept constant, the differential heat is the relevant quantity.

Experimentally, however, sorptional uptake measurements performed at different temperatures will provide the *integral* heat of solution as the composition of the polymer/gas mixture changes during the experiment. The experimental solubility coefficient[15] of the penetrant is often related to the sorption temperature by a Van't Hoff relation:[16]

$$S = S_0 \exp(-\Delta H_s/RT) \quad (7)$$

In eq 7, S is the solubility coefficient, S_0 is a constant, and ΔH_s is the integral heat of solution, which is assumed not to depend on temperature in the temperature window studied. When n_1 moles of the penetrant are dissolved in n_2 moles of the polymer, the integral heat of solution reads

$$\Delta H_s = n_1\Delta h_1 + n_2\Delta h_2 \quad (8)$$

In eq 8, Δh_1 is the partial molar enthalpy change of the gas ($\Delta h_1 = h_{ex}$), and Δh_2 is the partial molar enthalpy change of the polymer. Note that both quantities are functions of the composition variables n_1 and n_2. The experimentally obtained integral heat of solution will equal the differential heat of solution in the infinite-dilution limit ($\Delta n_1 \to 0$, n_2 constant); i.e., the differential, infinitesimal small process $\Delta n_1 \to 0$ justifies the assumption that the composition stays constant. Then, the partial molar enthalpy change of the polymer remains unaffected, i.e., $\Delta h_2 = 0$ and $\Delta H_s = n_1\Delta h_1$. Practically speaking, however, this argumentation can be questioned, because we cannot dissolve penetrants without changing the composition of the solution. Therefore, it remains important to still consider Δh_2 when attempting to relate ΔH_s to the partial thermodynamic property h_{ex} of the penetrant. Large penetrants will swell the polymer matrix, even at infinite dilution, causing the contribution Δh_2 in eq 8 to be nonnegligible and positive (due to decreased cohesion of the polymer). This effect can safely be assumed not to occur, however, when small-sized penetrants such as He and H_2 are dissolved at infinite dilution; i.e., the preexisting free volume pockets in the amorphous polymer are large enough to accommodate these penetrants without significant distortion of the polymer matrix.

From the discussion above it becomes clear that the experimental, integral heat of solution ΔH_s, obtained from eq 7, is related to the differential heat of solution (h_{ex}) according to $\Delta H_s = h_{ex} - RT$, provided that (1) h_{ex} and s_{ex} are constants in the temperature window that is being studied and (2) sorption of small-sized, noncondensable penetrants is studied in the infinite-dilution limit. The subtraction of RT is due to the (experimental) definition of the solubility.[15]

Because, in experiments (that apply eq 7 to obtain ΔH_s), it is difficult to verify whether the first condition has been met, ΔH_s is often referred to as the *apparent* heat of solution. Only when h_{ex} and s_{ex} are not affected by temperature do the apparent and true heat of solution become equal.

3. Model and Simulation Details

All simulations were performed using the GROMOS package.[17] The equations of motion were integrated with a leapfrog algorithm with a 4 fs integration time step. All polymer bond lengths were constrained using the SHAKE algorithm.[18] For the nonbonded interactions, a cutoff distance of 1.15 nm was used. An atomic pair list was used, which was updated every 10 time steps. Constant pressure and temperature dynamics was performed by weak coupling[19] to a pressure and temperature bath with coupling times 0.5 ps (pressure) and 0.1 ps (temperature).[19] The virial contribution to the pressure was long range corrected using an analytical expression based on the assumption that density correlations are absent beyond the cutoff distance.[20]

Polyethylene was modeled using a united atom force field described elsewhere.[12] The simulation boxes all contained 12 polyethylene chains, each consisting of 118 CH_2 groups and two CH_3 end groups. The polyethylene box was prepared by the slow compression method described in ref 12. The carbon dioxide molecule was modeled with a united atom potential with Lennard-Jones potential parameters $\epsilon/k_b = 236.1$ K and $\sigma = 0.372$ nm.[10] Parameters for unlike interactions were determined using Lorentz−Berthelot mixing rules.[20] To study penetrant diffusion, 10 CO_2 penetrants were introduced in the PE box described above.

Simulations were performed at constant pressure (0.1 MPa) and constant temperature. MD simulations were performed at temperatures between 260 and 560 K with 20 K intervals. The systems at different state points were equilibrated during 500 ps simulations, starting at the lowest temperature. At each new temperature, the initial set of coordinates and velocities was taken from the previous, lower temperature run. Equilibrated box volumes between 38.4 ± 0.3 nm^3 (260 K) and 47.5 ± 0.6 nm^3 (560 K) were obtained. Penetrant mean-square displacements were calculated from 7 ns production runs (260−340 K) and 2.5 ns production runs (360−

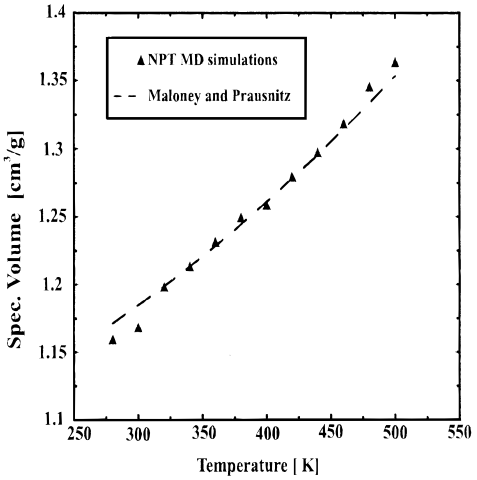

Figure 1. Specific volume (at 0.1 MPa) of PE vs temperature from MD simulation (triangles) compared with experiment.[22]

560 K), during which coordinates were stored every 1 ps. At all temperatures above 360 K, carbon dioxide excess chemical potentials were calculated from 1 ns trajectories of the penetrant-free (dry) polymer system. Below 360 K, 3 ns trajectories were used for this purpose. During these simulations 3.75×10^8 test-particle insertions were performed at the lower temperatures; 1.25×10^8 insertions were performed at the high temperatures.

4. Results

(a) *P*−*V*−*T* Behavior. To obtain reliable results for the diffusion and solubility coefficients of penetrants in polymeric matrices, it is very important to demonstrate that the host polymer itself is simulated reliably. Both the solubility and the diffusion of the penetrants are very sensitive to the free volume in the polymeric medium. Therefore, the volume−temperature properties at the pressure of interest must be realistically represented in the simulation. Figure 1 shows the $V-T$ behavior of the polyethylene melt at 0.1 MPa. The magnitude of the volume fluctuations was used to estimate the error on the individual points. At all temperatures this error was smaller than 0.02 cm^3/g. The coefficient of thermal volume expansion, a_T, is 8×10^{-4} K^{-1} (at 298 K) from the linearly fitted MD points, compared to 7.4×10^{-4} K^{-1} from experiment.[21] We have included in this figure the $V-T$ relation (0.1 MPa) experimentally determined by Maloney and Prausnitz.[22] Within the error of our calculations, the agreement is good.

(b) Penetrant Diffusion. Mean-Square Displacements. Figure 2 shows the mean-square displacement of the carbon dioxide diffusant at 300 K. At times smaller than 1000 ps the penetrant motion is highly anomalous; the linear regime—from which the diffusion coefficient is calculated—sets in at larger times. In the anomalous regime, collisional cage motions dominate the shape of the mean-square displacement curve. Intercavity jumps rarely occur at this time scale.[2,23] Figure 3 shows the carbon dioxide mean-square displacements at several temperatures above 400 K. Note the different time and length scales compared to the ones depicted in Figure 2. In the high-temperature mean-square displacement curves, the initial anomalous diffusion regime has disappeared (When the high-temperature mean-square displacement curves are plotted for times larger than 1 ns, no slope change occurs.) This indicates that the liquidlike transition has occurred. Diffusion coefficients are obtained from the slope of the curves at times smaller than 1000 ps.

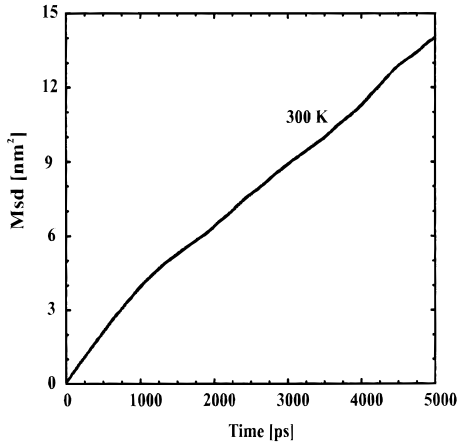

Figure 2. Penetrant mean-square-displacement (Msd) in PE at 300 K.

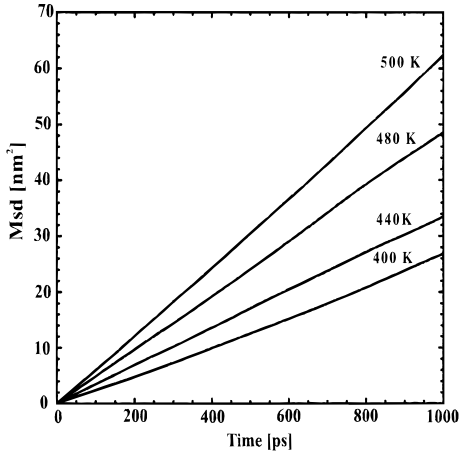

Figure 3. Penetrant mean-square-displacements (Msd) in PE at 400, 440, 480, and 500 K.

The transition from the hopping-diffusion regime into the liquidlike diffusion regime has been studied in detail by Pant and Boyd.[4] In this work, it was shown that the non-Arrhenius diffusion behavior manifests itself as a continuous transition, which is of WLF type.[4] To illustrate the transition in our simulations, we present several penetrant trajectories in Figure 4 projected two-dimensionally. The trajectory of a single penetrant is plotted at several temperatures during 1000 ps. At low temperatures (280 and 300 K) the penetrant spends most of its time exploring a free volume pocket and only rarely jumps to an adjacent pocket. At these temperatures, the free volume of the polymer is revealed from the plotted trajectories. At a higher temperature (380 K), the signature of the underlying free volume is gradually smeared out due to the increased dynamics of the polymer. At temperatures larger than 380 K, a random walk penetrant trajectory is observed, rendering the penetrant diffusion process liquidlike. The Arrhenius plot for diffusion is presented in Figure 5. We have performed linear fits (instead of a WLF fit) on the points below 380 K and the ones above 380 K to illustrate the slope change. The activation energy for diffusion equals $E_{act} = 23$ kJ/mol at low temperature and reduces to $E_{act} = 15$ kJ/mol at high temperatures. The activation energy at low temperatures is considerably lower than

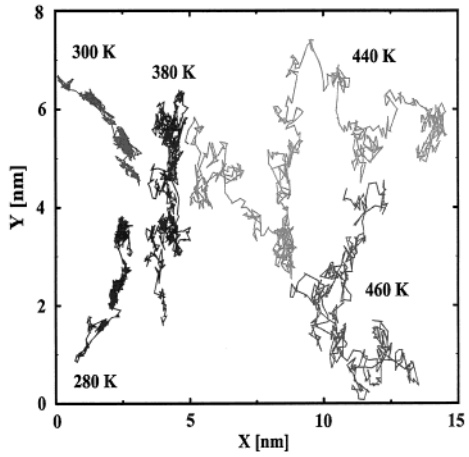

Figure 4. Single penetrant trajectories (1 ns) in PE at different temperatures.

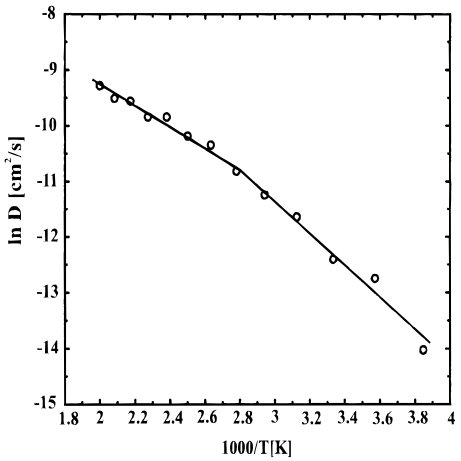

Figure 5. Arrhenius plot of the diffusion coefficient of carbon dioxide in PE from MD simulation (circles). Linear fits of the low-temperature and high-temperature regions are included to emphasize the slope change.

the one experimentally observed ($E_{act,exp}$ = 35.5 kJ/mol[24]) and than the one found by Pant and Boyd, who studied methane diffusion in PE.[4] This effect can most probably be attributed to the united atom description of our polymer/penetrant model. Previous simulations of polymer/penetrant systems using united atom descriptions of the interaction potential have all found to overestimate the speed of penetrant diffusion.[25,26]

(c) Carbon Dioxide Solubility. Carbon dioxide solubilities are presented in Figure 6. To estimate the statistical error on the individual solubility values presented in this figure, sets of block-averaged (uncorrelated) solubilities were calculated from the simulated trajectories. The separate blocks were chosen large enough to decorrelate the volume fluctuations of the simulated box, the process which took place within correlation times less than 50 ps (280 K). The standard deviations of the uncorrelated, block-averaged (50 ps) solubilities were found to lie between 1% of the penetrant solubility at 560 K and 6% of the penetrant solubility at 280 K. Figure 6 clearly reveals a strong non-Arrhenius behavior of the carbon dioxide solubility. To emphasize the change in slope, which occurs smoothly, we have included linear fits of the high-temperature (above 380 K) and the low-temperature (below 380 K) regions. Strikingly, the slope changes in the temperature range comparable to the one in the Arrhenius plot

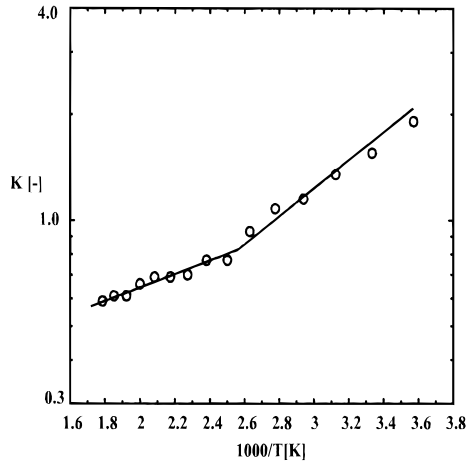

Figure 6. Arrhenius plot of the partition coefficient of carbon dioxide (at infinite dilution) in PE calculated from MD simulation (circles). Linear fits of the low-temperature and high-temperature regions are included to emphasize the slope change.

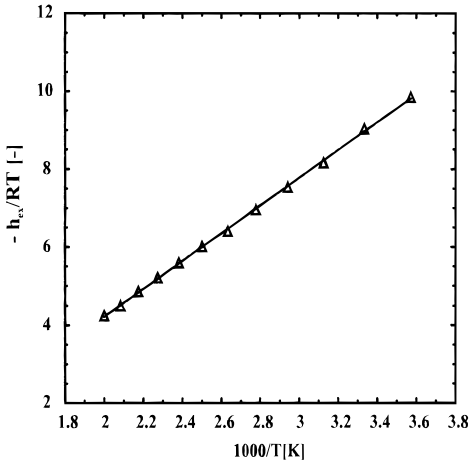

Figure 7. Excess partial molar enthalpy (units RT) of carbon dioxide in PE vs reciprocal temperature. The points obtained from MD simulation (triangles) were linearly fitted (solid line).

of the diffusivity. The (differential) apparent heat of solution, ΔH_s, obtained from a linear fit of the data in the low-temperature part (≤400 K) of Figure 6 and subsequent subtraction of RT (section 2b) equals −9.1 kJ/mol (298 K), which compares to the (integral) experimental value reported, −7.3 kJ/mol.[27] This comparison should be interpreted with some caution since the contribution of the partial molar enthalpy change of the polymer (Δh_2 section 2b) in the value obtained experimentally is unclear. MD simulations of the penetrant-free and the penetrant-containing system in principle allow to quantify Δh_2. In practice, however, a comparison of the enthalpy of these two systems is difficult because Δh_2 will be relatively small compared to the enthalpy fluctuations of the individual simulation boxes.

Partial Thermodynamic Properties. To investigate the change in slope in Figure 6, the excess partial molar enthalpy, $-h_{ex}/RT$, and entropy, s_{ex}/R, of the carbon dioxide penetrants are plotted in Figures 7 and 8, respectively, versus the reciprocal temperature. The sum of these two quantities reproduce the data points presented in Figure 6 (eq 6). The enthalpy contribution, $-h_{ex}/RT$, to the Arrhenius plot of the solubility grows linear with reciprocal temperature. This result leads us

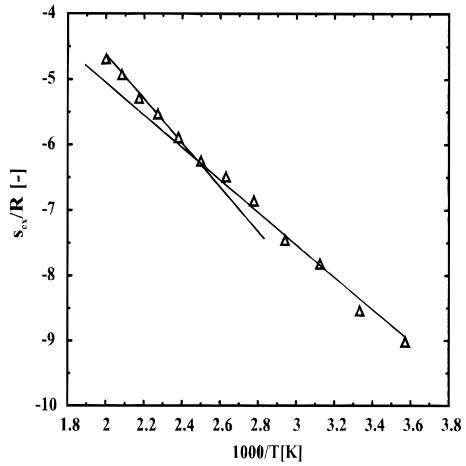

Figure 8. Excess partial molar entropy (units R) of carbon dioxide in PE vs reciprocal temperature (symbols). The low-temperature and high-temperature linear fits are extrapolated to emphasize the change in slope.

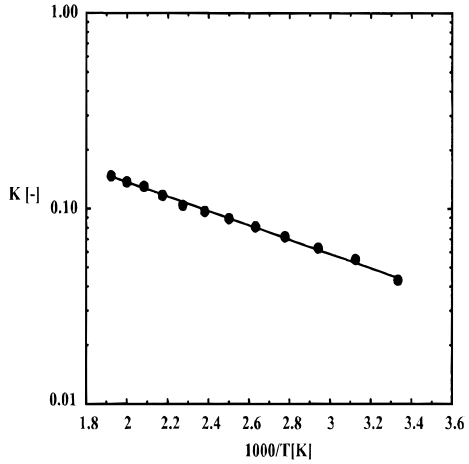

Figure 9. Arrhenius plot of the partition coefficient of helium (at infinite dilution) in PE from MD simulation (circles). The line is a linear fit of the data points. The partition coefficients were computed from 500 ps simulations during which 6.25×10^7 test-particle insertions were performed.

to conclude that changes in the excess partial molar enthalpy of the penetrant are not responsible for the slope change in Figure 6. The excess partial molar enthalpy h_{ex} equals −23.3 kJ/mol at 260 K and increases linearly to a value of −16.4 kJ/mol at 560 K (not shown). From Figure 8, it is seen that entropy is a strong increasing function of the sorption temperature, which, however, is not linear in $1/T$ but grows faster (with $1/T$ decreasing). To emphasize this, again two fits of the data points were included: one at temperatures $T > 380$ K and the other at temperatures $T \leq 380$ K. Despite the fact that the change in slope of the entropy is only weak, its effect on the penetrant solubility—obtained after addition of the data points in Figure 7—is significant. The change in slope in Figure 6 therefore is an entropic effect, which we will discuss in more detail in a later section.

Heat of Solution. The true heat of solution, h_{ex}, differs considerably (approximately by a factor 2−3) from the apparent heat of solution obtained from Figure 6, indicating that the latter quantity is strongly affected by entropy. Experimentally, apparent heats of solution of noncondensable gases (such as He and H_2) in various polymers have often found to be positive;[28] i.e., the solubility increases with increasing temperature. In studies of the solubility of gases in liquids, this effect has been explained[29] by dividing the heat of solution or enthalpy of sorption into two parts:

$$\Delta H_s = \Delta H_{cond} + \Delta H_{mix} \tag{9}$$

where ΔH_{cond} and ΔH_{mix} are the enthalpy changes associated with penetrant condensation and mixing, respectively. Because the enthalpy of a liquid is generally lower than that of a gas, ΔH_{cond} is negative. The enthalpy of mixing, ΔH_{mix}, tends to be positive; i.e., interactions between unlike molecules are usually less favorable than the ones between like molecules. In the absence of solvation between the gas penetrant and the solvent, the enthalpy of mixing can become strongly positive, dominating the contribution (eq 9) of condensation of the gas, rendering a positive enthalpy of sorption.

Similar arguments have been used to explain positive heats of solution for small, noncondensable gases in polymers.[28,30] On the basis of our results (Figures 7 and 8), it can be argued that for these gases the increase of entropy dominates the true heat of solution—which is negative (section 2b)—rendering the apparent heat positive. To test this hypothesis, we calculated the infinite-dilution helium solubility in our PE melt. Helium was treated as a Lennard-Jones atom with an energy well depth $\epsilon/k_b = 10$ K and diameter $\sigma = 0.26$ nm.[31] Figure 9 shows the Arrhenius plot of the helium solubility. The solubility is an increasing function of temperature; hence, the apparent heat of solution is positive. From the slope in Figure 9 we obtain (RT has again been subtracted) $\Delta H_s = 4.6$ kJ/mol (298 K). The experimental value is 5.9 kJ/mol.[32] The true heat of solution, h_{ex}, was calculated and equals −1.15 kJ/mol (300 K). At all temperatures studied, s_{ex}/R is a more rapidly growing function of temperature than $-h_{ex}/RT$ (not shown).

Distribution of Sorption Energies. The distribution of sorption energies in the polymer matrix, together with the actual population of these energies, provides a means to study the hoppinglike-to-liquidlike transition in more detail. Note that the actual population of energies is obtained from the product of the energy distribution and the Boltzmann factor. Structural inhomogeneities at spatial scales, including sparsely distributed low-energy sorption pockets and interpocket transition regions, will result in a broad distribution of penetrant energies. To facilitate the liquidlike diffusion process at high temperatures, an increasing number of neighboring sites with essentially identical (within k_bT) energies need to be homogeneously distributed and thermally accessible. We have investigated these features and have used the test-particle insertion energy to define the sorption energy distribution. We will present energy distributions instead of populations, since the first property is more sensitive to structural changes in the polymer matrix.

Figure 10 shows the test-particle energy distribution at several temperatures between 300 and 380 K. All distributions increase monotonically with energy with exception of the distribution at 380 K, which shows a weak maximum developing around −17 kJ/mol. At low energies (below −20 kJ/mol), all distributions grow rapidly; the higher energy parts show a gradual increase with energy. The excess partial molar enthalpies of the diffusant correspond to values in the low-energy tails

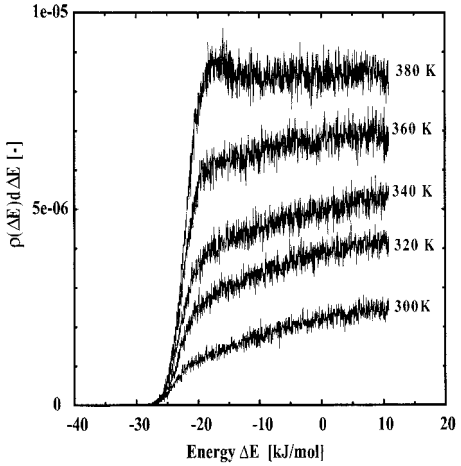

Figure 10. Distribution of test-particle insertion energies at several temperatures below 400 K. The energy scale presented does not include the high-energy parts (>10 kJ/mol) of the distributions.

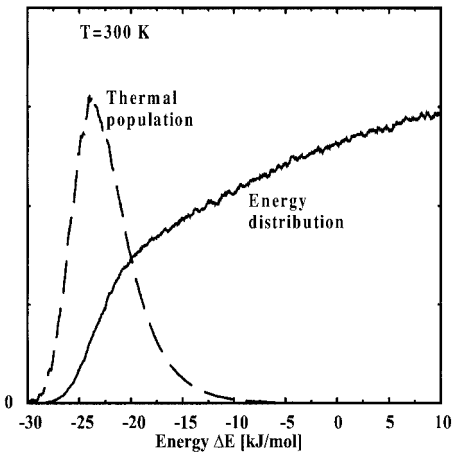

Figure 11. Distribution (solid line) and thermal population (dashed line) of penetrant energies in PE at 300 K. The thermal population and the energy distribution are rescaled vertically, to highlight the features of both functions.

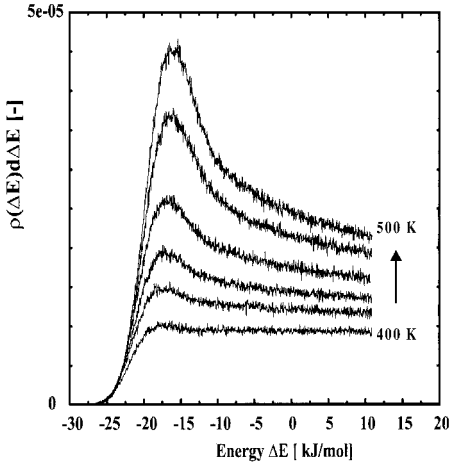

Figure 12. Distribution of test-particle insertion energies at temperatures 400, 420, 440, 460, 480, and 500 K. The energy scale presented does not include the high-energy parts (>10 kJ/mol) of the distributions.

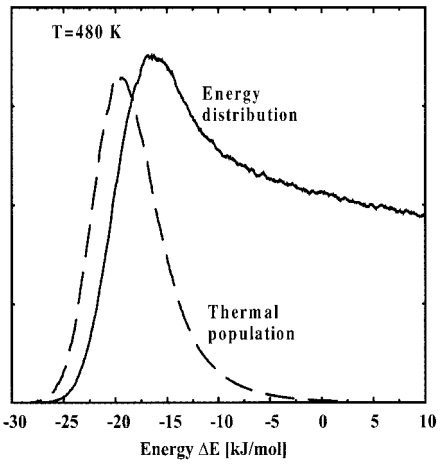

Figure 13. Distribution (solid line) and thermal population (dashed line) of penetrant energies in PE at 480 K. The thermal population and the energy distribution are rescaled vertically, to highlight the features of both functions.

of these distributions (Figure 7); i.e., at temperatures below 380 K, the low-energy sorption sites, sparsely distributed in the matrix, are populated. In Figure 11, we have plotted the energy distribution at 300 K together with the thermal population to illustrate this. Figure 12 shows the energy distributions at several temperatures higher than 380 K. All distributions show one broad prevailing peak, which was first developed at 380 K but now rises strongly and shifts to higher energies with increasing temperature. The excess partial molar enthalpies of the diffusants approximately match the various peak maxima (Figure 7). Therefore, at these temperatures the sorption sites, which are present in dominating amount, are being populated (see Figure 13). The shift in population—from penetrants occupying sparsely distributed low-energy sites to penetrants occupying sundry distributed higher-energy sites—will lower the activation zone for diffusion and explains the transition in the Arrhenius plot of the penetrant diffusion coefficient. The strongly growing number of available sorption sites at high temperatures causes the entropy of solution to grow increasingly rapid (Figure 8) and explains the non-Arrhenius behavior of the penetrant solubility (Figure 6).

5. Conclusion

From our MD simulations, we have shown that the permeability of polyethylene to carbon dioxide behaves strongly non-Arrhenius. This could be explained by a hoppinglike-to-liquidlike transition of the molecular-scale permeation mechanism of the penetrant. Sparsely distributed free volume pockets, with low sorption energies, were found populated at low temperatures. Consequently, the diffusional motions of the penetrant occurred by infrequent, strongly activated jumps between low-energy sites in the polymer matrix. At higher temperatures, a strongly increasing number of sorption sites with higher energy could be characterized. Moreover, the prevalent thermal population of these sites resulted in a decreased activation zone for diffusion and an increased entropy of solution. The latter causes a change in slope in the Arrhenius plot of the solubility, in the same temperature region where the activation energy for diffusion was found to decrease.

The apparent heat of solution, obtained from the Arrhenius plot of the penetrant solubility, is strongly affected by the temperature dependence of the entropy of solution. This caused the apparent heat to be significantly lower (less exothermic) than the true heat of

solution, at all temperatures studied. In addition, it was argued that this entropic effect might render the apparent heat of solution positive if noncondensable, small-sized penetrants are being dissolved in amorphous polymers.

In this paper, we have described the thermodynamic phenomena relating both the non-Arrhenius behaviors of the penetrant diffusion and solubility. The actual mechanistic processes must undoubtedly be searched for in the local dynamic and molecular packing features of the polymer.[4,5] Han and Boyd[5,33] and recently Bharadwaj and Boyd[34] have shown that small penetrant diffusion behaves strictly Arrhenius at even higher temperatures in polyisobutylene (PIB), atactic polystyrene (aPS), and aromatic polyesters. These findings probably reflect the inability of these polymers to redistribute free volume fast enough, in comparison to the diffusional motion of the penetrant. In high free volume polymers, e.g., polyethylene (PE), atactic polypropylene (aPP), and polybutadiene (PBD), the transition to liquidlike diffusion was clearly revealed.[35] In our work, changes in the penetrant diffusion and solubility coefficients were explained from the changes in the functional characteristics of the penetrant energy distribution $\rho(\Delta E)$. An important question to answer in future investigations is to what extent changes in the molecular packing nature, and free volume properties of the polymer, affect this distribution. In a subsequent paper, we will present free volume distributions of several polymeric melts and glasses, together with the solubilities of small molecular probes, to rationalize the microscopic changes that affect the penetrant energy distribution.

Acknowledgment. R. L. C. Akkermans is acknowledged for valuable comments.

References and Notes

(1) Stern, S. A. *J. Membr. Sci.* **1994**, *94*, 1.
(2) Gusev, A. A.; Müller-Plathe, F.; van Gunsteren, W. F.; Suter, U. W. *Adv. Polym. Sci.* **1994**, *116*, 207. Müller-Plathe, F. *Acta Polym.* **1994**, *45*, 259.
(3) Müller-Plathe, F.; Laaksonen, L.; van Gunsteren, W. F. *J. Mol. Graph.* **1993**, *11*, 118. Takeuchi, H. *J. Chem. Phys.* **1990**, *93*, 2062.
(4) Pant, P. V. K.; Boyd, R. H. *Macromolecules* **1993**, *26*, 679.
(5) Han, J.; Boyd, R. H. *Macromolecules* **1994**, *27*, 5365.
(6) Gusev, A. A.; Arizzi, S.; Suter, U. W. *J. Chem. Phys.* **1993**, *99*, 2221, 2228.
(7) Greenfield, M. L.; Theodorou, D. N. *Macromolecules* **1998**, *31*, 7068. Gray-Weale, A. A.; Henchman, R. H.; Gilbert, R. G.; Greenfield, M. L.; Theodorou, D. N. *Macromolecules* **1997**, *30*, 7296.
(8) When the gas-phase behaves nonideally, the excess chemical potential μ_{ex}^{gas} of the gas phase is included as well: $K = e^{-\mu_{ex}/RT} e^{\mu_{ex}^{gas}/RT}$. In this work we will consider the low-pressure, infinite-dilution solubility limit, in which the gas-phase behaves ideally.
(9) Widom, B. *J. Chem. Phys.* **1963**, *39*, 2802.
(10) Van der Vegt, N. F. A.; Briels, W. J.; Wessling, M.; Strathmann, H. *J. Chem. Phys.* **1999**, *110*, 11061.
(11) Müller-Plathe, F. *Macromolecules* **1991**, *24*, 6475.
(12) Van der Vegt, N. F. A.; Briels, W. J.; Wessling, M.; Strathmann, H. *J. Chem. Phys.* **1996**, *105*, 8849.
(13) Van der Vegt, N. F. A.; Briels, W. J. *J. Chem. Phys.* **1998**, *109*, 7578.
(14) Marrink, S.-J.; Berendsen, H. J. C. *J. Phys. Chem.* **1994**, *98*, 4155.
(15) Experimentally, the number density of penetrants sorbed in the polymer matrix is often presented relative to the number density of an ideal gas at standard conditions: $c = V(\mathrm{STP})/V \equiv Sp$, where $V(\mathrm{STP})$ denotes the volume of ideal gas at standard temperature and pressure: $T_0 = 273.15$ K and $P_0 = 1$ atm. This equation defines the solubility coefficient S, which is related to K as $S = (1/RT)(RT_0/P_0)K$.
(16) Kesting, R. E.; Fritzsche, A. K. *Polymeric Gas Separation Membranes*; Wiley: New York, 1993.
(17) Berendsen, H. J. C.; van Gunsteren, W. F. *GROMOS Reference Manual*; University of Groningen: Groningen, The Netherlands, 1987.
(18) Ryckaert, J.-P.; Ciccotti, G.; Berendsen, H. J. C. *J. Comput. Phys.* **1977**, *23*, 327.
(19) Berendsen, H. J. C.; Postma, J. P. M.; van Gunsteren, W. F.; Di Nola, A.; Haak, J. R. *J. Chem. Phys.* **1984**, *81*, 3684.
(20) Allen, M. P.; Tildesley, D. J. *Computer Simulation of Liquids*; Oxford Science Publishers: Oxford, UK, 1987.
(21) Brandrup, J., Immergut, E. H., Eds. *Polymer Handbook*, 2nd ed.; Wiley: New York, 1975.
(22) Maloney, D. P.; Prausnitz, J. M. *J. Appl. Polym. Sci.* **1974**, *18*, 2703.
(23) Takeuchi, H.; Okazaki, K. *Mol. Simul.* **1996**, *16*, 59.
(24) Michaels, A. S.; Bixler, H. J. *J. Polym. Sci.* **1961**, *L*, 413.
(25) Müller-Plathe, F.; Rogers, S. C.; van Gunsteren, W. F. *Macromolecules* **1992**, *25*, 6722.
(26) Müller-Plathe, F.; Rogers, S. C.; van Gunsteren, W. F. *Chem. Phys. Lett.* **1992**, *199*, 237.
(27) Hirose, T.; Mizoguchi, K.; Kamiya, Y. *J. Polym. Sci., Polym. Phys. Ed.* **1986**, *24*, 2107.
(28) Ghosal, K.; Freeman, B. D. *Polym. Adv. Technol.* **1994**, *5*, 673.
(29) Prausnitz, J. M. *Molecular Thermodynamics of Fluid Phase Equilibria*; Prentice Hall: Englewood Cliffs, NJ, 1986.
(30) Merkel, T. C.; Bondar, V.; Nagai, K.; Freeman, B. D.; Yampolskii, Yu. P. *Macromolecules* **1999**, *32*, 8427.
(31) Maitland, G. C.; Rigby, M.; Smith, E. B.; Wakehan, W. A. *Intermolecular Forces*; Clarendon: Oxford, UK, 1981.
(32) Michaels, A. S.; Bixler, H. J. *J. Polym. Sci.* **1961**, *L*, 393.
(33) Han, J.; Boyd, R. H. *Polymer* **1996**, *37*, 1797.
(34) Bharadwaj, R. K.; Boyd, R. H. *Polymer* **1999**, *40*, 4229.
(35) Gee, R. H.; Boyd, R. H. *Polymer* **1995**, *36*, 1435.

MA991737F